



Original Article

Characterizations of Cr³⁺-doped SnO₂ Powders Via a Hydrolysis Method

Trinh Thi Loan*, Vu Hoang Huong

VNU University of Science, 334 Nguyen Trai, Thanh Xuan, Hanoi, Vietnam

Received 17 April 2023

Revised 17 May 2023; Accepted 17 May 2023

Abstract: In this work, the effect of annealing temperature and Cr³⁺ concentration on the structural and optical properties of the SnO₂ host crystals has been investigated. The Cr-doped SnO₂ samples were synthesized by a simple hydrolysis method, using SnCl₄·5H₂O as the host precursor and CrCl₃·6H₂O as the source of dopant. X-ray diffraction and Raman scattering spectra analysis revealed a tetragonal rutile structure of Cr³⁺-doped SnO₂ samples. The Cr³⁺ concentration and annealing temperature have no influence on the lattice parameters of the SnO₂ crystals, whereas affected the appearance and intensity of the Raman modes. The optical properties of the synthesized samples were explored by photoluminescence (PL) and photoluminescence excitation (PLE) analysis. Interestingly, besides the emission peaks related to the SnO₂, emission transitions within Cr³⁺ ions in the octahedral field of SnO₂ were observed.

Keywords: SnO₂:Cr³⁺, hydrolysis, Raman, photoluminescence.

1. Introduction

SnO₂ is one of the important semiconducting oxides, due to its attractive properties like optical transmittance, uniformity, low resistivity, mechanical hardness, stability to heat treatment and piezoelectric behavior. SnO₂, an *n*-type wide band gap ($E_g = 3.6$ eV, at 300 K) semiconductor with an appreciable degree of ionicity, is attractive for many applications such as gas sensors [1], catalyst supports [2], dye-sensitized solar cells (DSSCs) [3], supercapacitors [4], transparent conducting electrodes [5]. Recently, to improve the properties and applicability of SnO₂, some researchers added the addition of metal or halogen ions as impurities, which are found to play an important role in changing the surface states, the electronic structure, the optical properties, etc. [2, 6, 7]. SnO₂ has been prepared

* Corresponding author.

E-mail address: loan.trinhthi@gmail.com

<https://doi.org/10.25073/2588-1124/vnumap.4845>

by various techniques such as chemical co-precipitation [8], hydrothermal [9], thermal evaporation [10], and RF sputtering process [11]. In this work, Cr^{3+} -doped SnO_2 samples were synthesized by the simple hydrolysis method to clarify the influence of Cr^{3+} ions on the structural and optical properties of SnO_2 host crystals.

2. Experimental

Cr^{3+} -doped SnO_2 samples were synthesized by a simple hydrolysis method, using $\text{SnCl}_4 \cdot 5\text{H}_2\text{O}$ as the host precursor and CrCl_3 aqueous solution as the source of dopant. The samples were prepared using hydrolysis in alcohol and solutions. In a typical synthesis, 2.5 g of $\text{SnCl}_2 \cdot 2\text{H}_2\text{O}$ salts were dissolved in 30 ml ethanol solution by stirring, followed by the addition of 30 ml distilled water into the solution. Then, an appropriate quantity of 0.02M solution of CrCl_3 was added to the above mixture under steady stirring conditions for 15 min. Then concentrated NH_4OH was added drop by drop to the solution until the pH value reached about 7, at which point the precipitate was observed. Thereafter, the precipitate was filtered and washed with distilled water. Finally, the precipitate was annealed at 700 °C and 1200 °C in the air for 3 hours.

The crystalline structure of Cr^{3+} -doped SnO_2 was checked on an Empyrean X-ray diffractometer (XRD), using $\text{Cu-K}\alpha 1$ irradiation ($\lambda = 1.54056 \text{ \AA}$). Raman spectra were measured on LabRam HR800 (Horiba) spectrometer with 632.8 nm excitation. The PL and PLE spectra were recorded at room temperature on a Fluorolog FL3-22 (Jobin Yvon Spex) spectrofluorometer with a xenon lamp of 450 W as an excitation source.

3. Results and Discussion

3.1. Structure Characterization

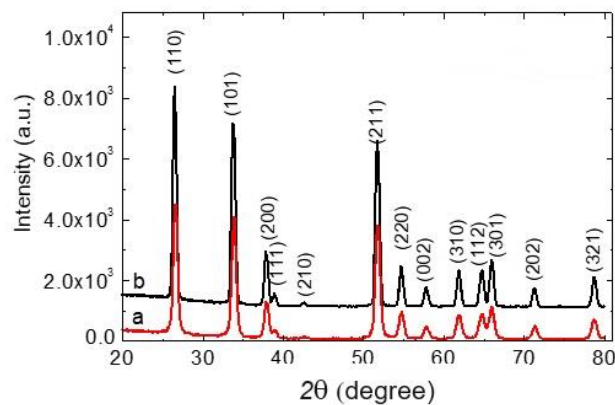


Figure 1. XRD patterns of undoped samples annealed at different temperatures for 3 hours: (a)- 700 °C and (b)- 1200 °C.

Fig. 1 shows XRD patterns of the undoped SnO_2 samples annealed at 700 and 1200 °C in the air for 3 hours. It is clearly seen that the positions of the diffraction peaks are independent of the annealing temperature. However, when increasing annealing temperature, the diffraction peaks became sharper and stronger, which indicated an increase in crystalline grain size of the samples, namely the

improvement of the crystallinity. All the samples exhibited the characteristic peaks corresponding to the (110), (101), (200), (111), (210), (211), (220), (002), (310), (112), (301), (202) and (321) planes at 26.7°, 33.8°, 37.9°, 39.1°, 42.7°, 51.8°, 54.7°, 57.9°, 61.9°, 64.8°, 65.9°, 71.3° and 78.8°, respectively, of rutile tetragonal SnO₂ structure (JCPDS No. 21-1250). The calculated lattice parameters of the unit cell are $a = b = 4.763 \pm 0.028 \text{ \AA}$ and $c = 3.194 \pm 0.007 \text{ \AA}$ ($\alpha = \beta = \gamma = 90^\circ$), in rather good agreement with the standard values $a = b = 4.73800 \text{ \AA}$, $c = 3.18800 \text{ \AA}$ (JCPDS No. 21-1250). The average crystallite grain sizes of SnO₂ nanostructures were determined by Sherrer's formula [8] and estimated to be ca. 14 nm and 20 nm in samples annealed at 700 and 1200 °C, respectively.

To find out the effect of Cr³⁺ dopant concentration on the crystalline structure of the synthesized samples, XRD patterns of Cr³⁺-SnO₂ powders with 0, 1, 3, 6, and 9 mol% Cr³⁺, annealed at 1200 °C in 3 hours were done, the results are shown in Fig. 2. Similar to the undoped sample, the samples doped with 1 mol% Cr³⁺ exhibits a rutile tetragonal SnO₂ (pattern "b" in Fig. 2). There are no other crystalline phases observed. However, in the XRD patterns of the SnO₂ powders doped with 3.0, 6.0 and 9.0 mol% Cr³⁺ (patterns "c", "d", and "e" in Fig. 2) apart from the characteristic peaks of the rutile phase, three weak peaks of α-Cr₂O₃ at 2θ of 24.4°, 36.3° and 50.2° corresponding to (012), (110), and (024) planes [12], were revealed respectively. The interplanar spacing (d) and calculated lattice parameters (a, c) of the synthesized samples are listed in Table 1. It is well known that in octahedral coordination, the effective ionic radius of Cr³⁺(0.62 Å) is close to that of host Sn⁴⁺ ions (0.69 Å). Hence with a relatively low Cr³⁺ doping content incorporated into SnO₂ crystalline, the lattice parameters within the error limits remain almost unchanged and independent on Cr³⁺ content.

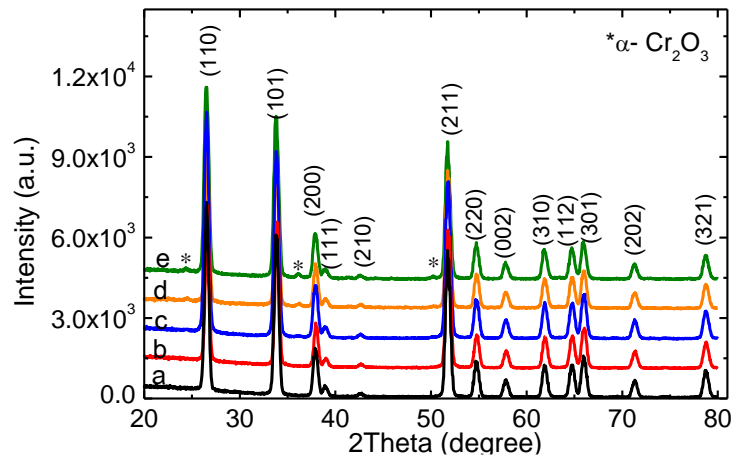


Figure 2. XRD patterns of SnO₂:Cr³⁺ samples as a function of doping concentration: (a) 0 mol%, (b) 1 mol%, (c) 3 mol%, (d) 6 mol%, and (e) 9 mol%.

Table 1. The lattice parameters of SnO₂:Cr³⁺ samples with different doping concentrations.

Cr ³⁺ content (% mol)	d ₁₁₀ (Å)	d ₁₀₁ (Å)	d ₂₁₁ (Å)	The lattice parameters (Å)	
				a = b	c
0	3.368	2.653	1.771	4.763 ± 0.028	3.194 ± 0.007
1	3.356	2.648	1.771	4.746 ± 0.004	3.191 ± 0.003
3	3.368	2.653	1.767	4.763 ± 0.004	3.194 ± 0.006
6	3.356	2.653	1.771	4.746 ± 0.005	3.200 ± 0.006
9	3.368	2.653	1.771	4.763 ± 0.028	3.194 ± 0.006

Raman scattering characterization provides information on the structural disorder on the material surface. Rutile SnO₂ belongs to the point group D_{4h} ¹⁴ and space group PA_2/mnm . According to the group theory, SnO₂ in its rutile phase generates 18 branches for the vibration modes in the first Brillouin zone. Two modes are infrared active (the single A_{2u} and the triply degenerate E_u), four modes are Raman active (the three nondegenerate A_{1g} , B_{1g} , B_{2g} modes and the doubly degenerate E_g one) and two others are silent (the A_{2g} and B_{1u} modes).

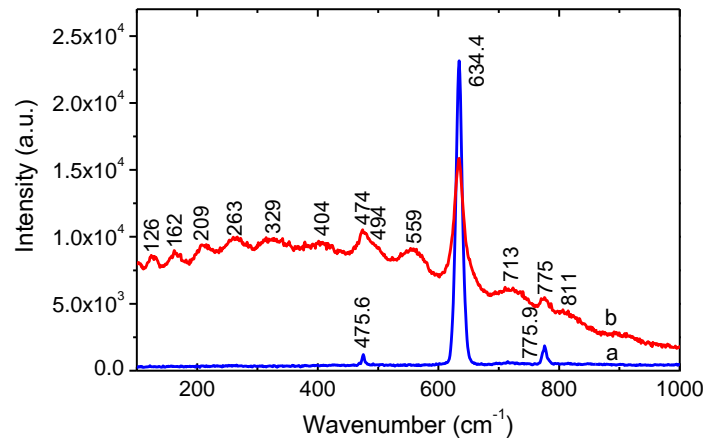


Figure 3. Raman spectra of the undoped SnO₂ samples annealed at different temperatures: (a)- 1200 °C and (b)- 700 °C.

For comparison, the Raman spectra of the undoped SnO₂ samples annealed at 700 and 1200 °C are investigated and depicted in Fig. 3. The spectrum of the undoped sample annealed at 1200 °C (line "a" in Fig. 3) is characterized by the presence of three peaks located at about 475.6, 634.4 and 775.9 cm⁻¹, with an intense peak at 634.4 cm⁻¹. These peaks correspond to the E_g , A_{1g} and B_{2g} fundamental phonon modes, respectively, in good agreement with those observed in a pure SnO₂ [13]. It is well known that the doubly degenerate E_g mode relates to the vibration of oxygen in the oxygen plane, whereas the nondegenerate A_{1g} and B_{2g} Raman modes denote the contraction and expansion of the vibrating mode of Sn–O bonds [13]. Unlike the samples annealed at 1200 °C, in the Raman spectrum of the undoped sample annealed at 700 °C, ten weak peaks at 126, 162, 209, 263, 329, 404, 494, 559, 713, and 811 cm⁻¹ were observed except the peaks of E_g (474 cm⁻¹), A_{1g} (634.4 cm⁻¹) and B_{2g} (775 cm⁻¹). The reasons why these Raman modes appeared are related to decreasing size and increasing disorder by lower annealing temperatures. It is interesting to know that Raman silent modes, the IR active modes and optically inactive modes transform to a Raman active mode owing to the size effect and the presence of oxygen vacancies [14]. The vibrational peak at 126 cm⁻¹ is attributed to the B_{1g} [15, 16]. The peaks at 494 cm⁻¹ and 713 cm⁻¹ may be assigned as $A_{2u}(TO)$ and $A_{2u}(LO)$ (namely, TO is the mode of the transverse optical phonons, LO is the mode of the longitudinal optical phonons) modes [17-19]. The peaks at 209, 263 and 329 cm⁻¹ might be corresponded to the $E_u(1)(TO)$, $E_u(1)(LO)$ and $E_u(2)(LO)$, respectively [19, 20]. The peaks at 559 and 812 cm⁻¹ may be related to surface defects of the SnO₂ nanocrystals [21, 22]. Two peaks at 162 and 404 cm⁻¹ can be assigned to the forbidden Raman modes B_{1u} and A_{2g} , respectively [23].

The Raman spectra of the SnO₂ samples doped with different Cr³⁺ concentration, annealed at 1200 °C for 3 hours are shown in Fig. 4. In general, the intensities of the Raman modes gradually decrease with the increase of Cr³⁺ concentration. The reduction of the Raman modes intensity when

doping Cr^{3+} can be considered as a proof of the incorporation of Cr^{3+} within the SnO_2 lattice. It is noteworthy that, compared with the undoped sample, the Raman spectra of the Cr^{3+} -doped SnO_2 powders exhibit some new peaks at 161, 603 and 713 cm^{-1} . These peaks clearly appeared in the Raman spectra of the samples with Cr^{3+} contents of 1.0 and 3.0 mol%. As above stated, the two peaks at 161 and 713 cm^{-1} are assigned to Raman modes B_{1u} and $A_{2u}(\text{LO})$, respectively. The peak at 603 cm^{-1} corresponds to the $E_u(3)(\text{TO})$ [19]. The observation of these new peaks can be attributed to the effect of the disorder crystalline structure associated with Cr^{3+} doping. The Cr^{3+} dopant slightly changes the defects and local disorders like vacant lattice sites in SnO_2 host crystals, which may result in the breakdown of the phonon momentum selection rule $q_0 \approx 0$ is well expected, and the contribution of phonons with $q \neq 0$ to the Raman spectrum is allowed.

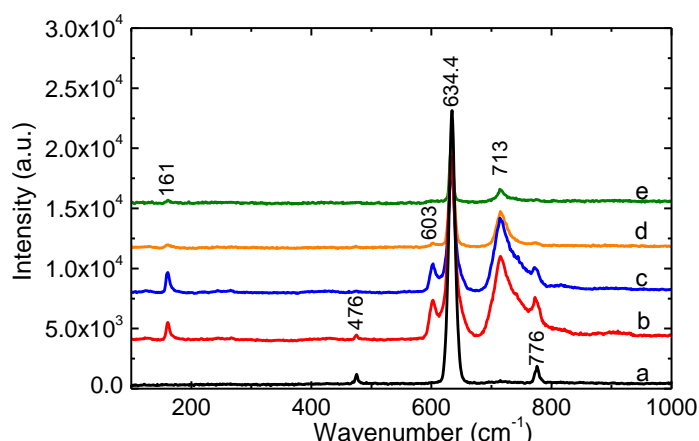


Figure 4. Raman spectra of $\text{SnO}_2:\text{Cr}^{3+}$ samples with different doping concentrations, annealed at 1200 °C in 3 h: (a)- 0 mol%, (b)- 1 mol%, (c)- 3 mol%, (d)- 6 mol% and (e)-9 mol%.

3.2. Optical Characterization

It is well known that the PL emission spectra reveal the extent of charge carrier trapping, transfer, and migration of interfacial photogenerated charge pair in a semiconductor material. Basically, the PL spectrum of rutile SnO_2 resulted from three origins: NBE emission; surface dangling bonds or oxygen vacancies and Sn interstitials; and doubly ionized oxygen vacancies [20]. Fig. 5 presents PL spectra acquired at room temperature, excited by 280 nm wavelength of the $\text{SnO}_2:\text{Cr}^{3+}$ samples with different doping concentrations, annealed at 1200 °C in 3 hours. The undoped sample has a prominent broad band peaking at 434 nm and another weak band peaking at 352 nm (line "a" in Fig. 5). The doped samples have similar bands but with weaker intensity. From Fig. 5, it can be seen that for the undoped sample, the ratio of the intensity of the visible emission to the UV emission is very large, whereas, for the doped sample, this ratio is insignificant. The peak at 352 nm is not due to band edge emission because SnO_2 is a direct bandgap semiconductor. However, limited by its dipole-forbidden nature, the bandgap emission is prohibited at room temperature due to the selection rule [25]. Therefore, according to previous works, the peak at 352 nm is assigned as NBE emission [21]. As shown in the inset of Fig. 5, the band emission in about 375-500 nm of Cr^{3+} -doped SnO_2 samples consists of the peaks at 398, 421, 436, 450, 468, 482, and 496 nm. The peak at 398 nm is attributed to luminescence centers as crystalline structure defects [26]. Three peaks at 421 nm, 436 nm, and 450 nm are associated with surface dangling bonds or oxygen vacancies and Sn interstitials [21, 24]. Three peaks at 468 nm, 482 nm, and 496 nm are due to doubly ionized oxygen vacancies [21].

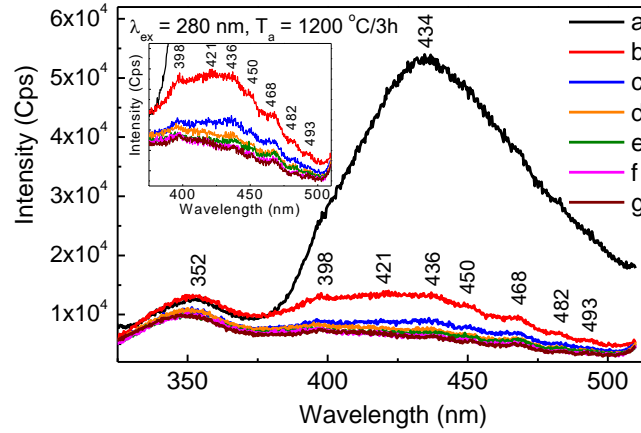


Figure 5. PL spectra excited by 280 nm wavelength of the $\text{SnO}_2:\text{Cr}^{3+}$ samples with different doping concentrations, annealed at 1200 °C in 3 h: (a)- 0 mol%, (b)- 0.1 mol%, (c)- 0.5 mol%, (d)- 1 mol%, (e)- 3 mol%, (f)- 6 mol% and (g)- 9 mol%.

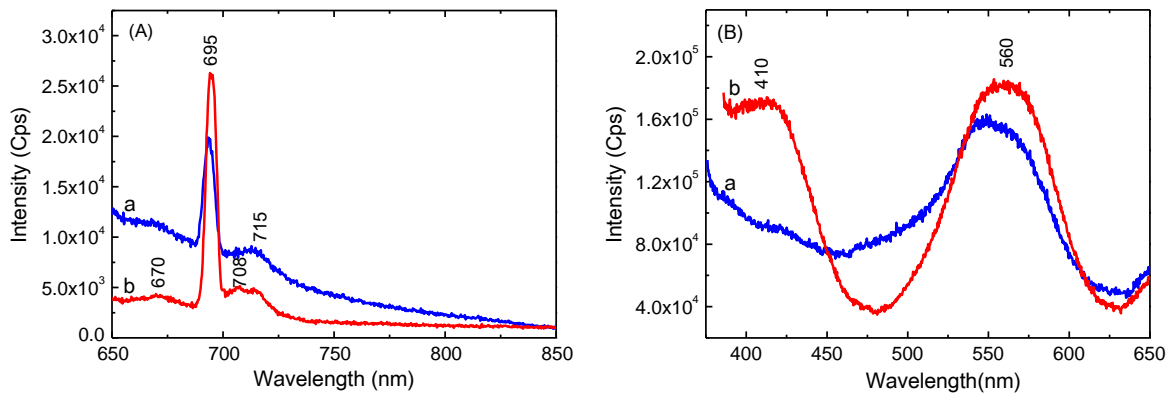


Figure 6. PL (A) and PLE (B) spectra of the $\text{SnO}_2:\text{Cr}^{3+}$ samples doped with 0.1 mol% annealed at different temperatures in 3 h: (a) 700 °C and (b) 1200 °C.

Fig. 6 presents the PL and PLE spectra of the $\text{SnO}_2:\text{Cr}^{3+}$ samples doped with 0.1 mol% annealed at 700 and 1200 °C for 3 h. It can be clearly seen that the PL and PLE spectra of the sample annealed at 700 °C are similar to the one of the sample annealed at 1200 °C, except weaker intensity. As shown in Fig. 6A, the PL spectrum excited by 560 nm wavelengths of the sample annealed at 1200 °C consists of a very prominent narrow emission peak at 695 nm and three weaker peaks at 670, 708, and 715 nm. The emission peak at 695 nm is believed to be related to the transition from the ${}^2E({}^2G)$ excited state to the ${}^4A_2({}^4F)$ ground state within Cr^{3+} ions located in the octahedral field of SnO_2 host and very weak peaks at 670, 708, 715 nm being its phonon-sidebands [26, 27]. The PLE spectrum of the sample annealed at 1200 °C and monitored at 695 nm exhibits two bands in the 375-475 nm and 475-625 nm ranges with peak positions of ≈ 410 nm and ≈ 560 nm, respectively. Two bands with the peak position of ≈ 410 nm and ≈ 560 nm correspond to ${}^4A_2({}^4F) \rightarrow {}^4T_1({}^4F)$ and ${}^4A_2({}^4F) \rightarrow {}^4T_2({}^4F)$ transitions within Cr^{3+} ions located in the octahedral field of SnO_2 host, respectively. From this result, one can suggest that Cr^{3+} ions were properly incorporated into the SnO_2 host lattice.

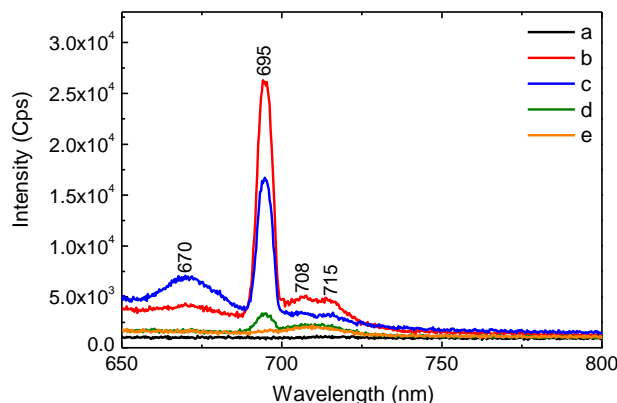


Figure 7. PL spectra of the $\text{SnO}_2:\text{Cr}^{3+}$ samples doped with different doping concentrations, annealed at 1200°C in 3h: (a)- 0 mol%, (b)- 0.1 mol%, (c)- 0.5 mol%, (d)- 1 mol%, (e)- 3 mol%.

To study the effects of Cr^{3+} contents on the properties optical, the PL spectra excited by 560 nm wavelengths of the anatase SnO_2 samples doped with different Cr^{3+} concentrations were recorded, as shown in Fig. 7. It can be seen that undoped samples do not emit light in the wavelength range of 650-800 nm (line "a" in Fig. 7). This confirms that the peaks 670, 695, 708 and 715 nm belong to the emissions of Cr^{3+} ions located in the octahedral field of the SnO_2 host. Besides, the SnO_2 sample doped with 0.1 mol% Cr^{3+} has the strongest emission intensity. The obtained PL spectra shown Fig. 5 and Fig. 7 demonstrate that the intensity of all emission peaks decreases with the increase of the doping concentration, which can be attributed to the decrease in the rate of recombination for electron-hole pairs due to increasing Cr^{3+} content.

4. Conclusion

SnO_2 powders doped with different Cr^{3+} concentrations of (from 0 to 9 mol%) were prepared by a simple hydrolysis method. According to the XRD analysis, the obtained samples have single SnO_2 crystalline phase when doping with a Cr^{3+} concentration lower 1.0 mol%. With doping concentrations above 3.0 mol%, in the samples $\alpha\text{-Cr}_2\text{O}_3$ appeared. The annealing temperature as well as the doping concentration have a significant influence on both the appearance and the intensity of the characteristic Raman modes of the SnO_2 host lattice. Some forbidden Raman and infrared active modes such as B_{1u} , A_{2g} , A_{2u} and E_u of undoped samples annealed at 700°C and Cr-doped SnO_2 were observed. The PL of the Cr^{3+} -doped SnO_2 consists of two groups of emission bands, one in 325-500 nm range related to the SnO_2 host, another in 650-750 nm range related to ${}^2E({}^2G) \rightarrow {}^4A_2({}^4F)$ transitions within Cr^{3+} ions in the octahedral field of SnO_2 . In PLE of Cr^{3+} -doped SnO_2 , the peaks related to ${}^4A_2({}^4F) \rightarrow {}^4T_1({}^4F)$ and ${}^4A_2({}^4F) \rightarrow {}^4T_2({}^4F)$ transitions within Cr^{3+} ions located in the octahedral field of SnO_2 host lattice were observed. From the obtained results, one can expect to the potential applications of the Cr^{3+} -doped SnO_2 materials, in solid-state lighting, in particular.

References

- [1] K. Shehzad, N. A. Shah, M. Amin, M. Abbas, W. A. Syed, Synthesis of SnO_2 Nanowires for CO, CH_4 and CH_3OH Gases Sensing, Int. J. Distrib. Sens. Netw., Vol. 14, No. 8, 2018, pp. 1-10, <https://doi.org/10.1177/1550147718790750>.

- [2] S. G. Lee, S. B. Han, W. J. Lee, K. W. Park, Effect of Sb-Doped SnO₂ Nanostructures on Electrocatalytic Performance of a Pt Catalyst for Methanol Oxidation Reaction, *Catalysts*, Vol. 10, No. 8, 2020, pp. 2-15, <https://doi.org/10.3390/catal10080866>.
- [3] N. N. Dinh, M. C. Bernard, A. H. Goff, T. Stergiopoulos, P. Falaras, Photoelectrochemical Solar Cells Based on SnO₂ Nanocrystalline Films, *C. R. Chimie*, Vol. 9, No. 5-6, 2006, pp. 676-683, <https://doi.org/10.1016/j.crci.2005.02.042>.
- [4] K. Manikandan, S. Dhanuskodi, N. Maheswari, G. Muralidharan, SnO₂ Nanoparticles for Supercapacitor Application, *AIP Conference Proceedings*, Vol. 1731, No. 050048, 2016, pp. 1-3, <http://dx.doi.org/10.1063.4947702>.
- [5] Ginley, S. David, Transparent Conducting Oxides Based on Tin Oxide, R. Kykyneshi, J. Zeng, D. P. Cann, *Handbook of Transparent Conductors*, 2011, pp. 171-191, <http://dx.doi.org/10.1007/978-1-4419-1638-96>.
- [6] Bhawna, A. K. Choudhary, A. Gupta, S. Kumar, P. Kumar, R. P. Singh, V. Kumar, Synthesis, Antimicrobial Activity, and Photocatalytic Performance of Ce Doped SnO₂ Nanoparticles. *Front. Nanosci.*, Vol. 2, No. 595352, 2020, pp. 1-7, <http://dx.doi.org/10.3389/fnano.2020.595352>.
- [7] P. P. Filippatos, N. Kelaidis, M. Vasilopoulou, D. Davazoglou, A. Chroneos, Defect Processes in Halogen Doped SnO₂, *Appl. Sci*, Vol. 11, No. 2, 2021, pp. 1-14, <https://doi.org/10.3390/app11020551>.
- [8] S. Naz, I. Javid, S. Konwar, K. Surana, P. K. Singh, M. Sahni, B. Bhattacharya, A Simple Low-cost Method for Synthesis of SnO₂ Nanoparticles and Its Characterization, *SN Appl. Sci*, Vol. 2, No. 5, 2020, <https://doi.org/10.1007/s42452-020-2812-2>.
- [9] F. Zahmatkeshani, M. Tohidi, Synthesis of SnO₂, Zn-doped SnO₂ and Zn₂SnO₄ Nanostructure-based Hierarchical Architectures by using Deep Eutectic Precursors and their Photocatalytic Application. *Cryst. Eng. Comm*, Vol. 21, 2019, pp. 6758-6771, <https://doi.org/10.1039/c9ce00886a>.
- [10] G. H. Lee, Change in the Morphology of SnO₂ Crystals Synthesized by Thermal Evaporation of SnO₂ Powder Mixed with Graphite in Ambient Air, *J. Ceram. Soc. JAPAN*, Vol. 126, No. 7, 2018, pp. 547-550, <http://doi.org/10.2109/jcersj2.18047>.
- [11] A. K. Gangwar, R. Godiwal, J. Jaiswal, V. Baloria, P. Pal, G. Gupta, & P. Singh, Magnetron Configurations Dependent Surface Properties of SnO₂ Thin Films Deposited by Sputtering Process, *Vacuum*, Vol. 177, No. 109353, 2020, <http://doi.org/10.1016/j.vacuum.2020.109353>.
- [12] B. T. Sone, E. Manikandan, A. G. Fakim, M. Maaza, Single-phase α-Cr₂O₃ Nanoparticles' Green Synthesis using Callistemon Viminalis' Red Flower Extract, *Green Chem. Lett. Rev*, Vol. 9, No. 2, 2016, pp. 85-90, <https://doi.org/10.1080/17518253.2016.1151083>.
- [13] S. Asaithambi, P. Sakthivel, M. Karuppaiah, Y. Hayakawa, A. Loganathan, G. Ravi, Improved Photocatalytic Performance of Nanostructured SnO₂ Via Addition of Alkaline Earth Metals (Ba²⁺, Ca²⁺ and Mg²⁺) under Visible Light Irradiation. *Appl. Phys. A*, Vol. 126, No. 4, 2020, pp. 1-12, <https://doi.org/10.1007/s00339-020-3441-8>.
- [14] A. Loganathan, D. Manoharan, N. V. Jaya, Defect Structure and Optical Phonon Confinement in Ultrananocrystalline Bi_xSn_{1-x}O₂ (x = 0, 0.03, 0.05, 0.08) Synthesized by Sonochemical Method, *Phys. Chem. Chem. Phys.*, Vol. 18, 2016, pp. 5995-6004, <https://doi.org/10.1039/C5CP06214D>.
- [15] P. S. Peercy, B. Morosin, Pressure and Temperature Dependences of the Raman-Active Phonons in SnO₂, *Phys. Rev. B*, Vol. 7, No. 2779, 1973, pp. 2779-2786, <https://doi.org/10.1103/PhysRevB.7.2779>.
- [16] F. Medjaldi, A. Bouabellou, Y. Bouachiba, A. Taabouche, K. Bouatia, H. Serrar, Study of TiO₂, SnO₂ and Nanocomposites TiO₂:SnO₂ Thin Films Prepared by Sol-gel Method: Successful Elaboration of Variable-refractive Index Systems, *Mater. Res. Express*, Vol. 7, No. 016439, 2020, <https://doi.org/10.1088/2053-1591/ab6c0c>.
- [17] N. Salah, S. Habib, A. Azam, M. S. Ansari, W. M. A. Shawafi, Formation of Mn-doped SnO₂ Nanoparticles Via the Microwave Technique: Structural, Optical and Electrical Properties, *Nanomater. Nanotechnol*, 2016, <https://doi.org/10.5772/62520>.
- [18] A. Diéguez, A. R. Rodríguez, A. Vilà, J. R. Morante, The Complete Raman Spectrum of Nanometric SnO₂ Particles. *J. Appl. Phys.*, Vol. 90, No. 3, 2001, pp. 1550-1557, <https://doi.org/10.1063/1.1385573>.
- [19] S. Roy, A. G. Joshi, S. Chatterjee, A. K. Ghosh, Local Symmetry Breaking in SnO₂ Nanocrystals with Cobalt Doping and Its Effect on the Optical Properties, *Nanoscale*, Vol. 10, No. 22, 2018, pp. 10664-10682, <https://doi.org/10.1039/C7NR07427A>.

- [20] N. Ahmad, S. Khan, M. M. N. Ansari, Exploration of Raman Spectroscopy, Dielectric and Magnetic Properties of (Mn, Co) Co-doped SnO₂ Nanoparticles, *Phys. Rev. B Condens. Matter*, Vol. 558, 2019, pp. 131-141, <https://doi.org/10.1016/j.physb.2019.01.044>.
- [21] N. Bhardwaj, S. Kuriakose, S. Mohapatra, Structural and Optical Properties of SnO₂ Nanotowers and Interconnected Nanowires Prepared by Carbothermal Reduction Method, *J. Alloys Compd*, Vol. 592, 2014, pp. 238-243, <https://doi.org/10.1016/j.jallcom.2013.12.268>.
- [22] W. B. H. Othmen, B. Sieber, H. Elhouichet, A. Addad, B. Gelloz, M. Moreau, S. Szunerits, R. Boukherroub, Effect of High Fe Doping on Raman Modes and Optical Properties of Hydrothermally Prepared SnO₂ Nanoparticles, *Materials Science in Semiconductor Processing*, Vol. 77, 2018, pp. 31-309, <https://doi.org/10.1016/j.mssp.2017.12.014>.
- [23] T. Lan, C. W. Li, B. Fultz, Phonon Anharmonicity of Rutile SnO₂ Studied by Raman Spectrometry and First Principles Calculations of the Kinematics of Phonon-phonon Interactions, *Phys. Rev. B*, Vol. 86, No. 13, 2012, pp. 134302_1-134302_7, <https://doi.org/10.1103/PhysRevB.86.134302>.
- [24] T. T. Loan, N. N. Long, Synthesis and Characterization of Ni²⁺-doped SnO₂ Powders, *VNU Journal of Science: Mathematics – Physics*, Vol. 35, No. 4, 2019, pp. 33-40, <https://doi.org/10.25073/2588-1124/vnumap.4356>.
- [25] R. Liu, Y. Chen, F. Wang, L. Cao, A. Pan, G. Yang, T. Wang, B. Zou, Stimulated Emission from Trapped Excitons in SnO₂ Nanowires, *Physica E*, Vol. 39, No. 2, 2007, pp. 223-229, <https://doi.org/10.1016/j.physe.2007.04.009>.
- [26] T. T. Loan, N. N. Long, Synthesis and Optical Properties of ZnAl₂O₄/Al₂O₃:Cr³⁺ Composite Materials, *VNU Journal of Science: Mathematics – Physics*, Vol. 34, No. 1, 2018, pp. 1-7, <https://doi.org/10.25073/2588-1124/vnumap.4253>.
- [27] T. T. Loan, N. A. Bang, V. H. Huong, N. N. Long, Effect of Cr³⁺ Concentration on Structural and Optical Properties of TiO₂:Cr³⁺ Anatase and Rutile Phases, *Opt. Mater*, Vol. 69, 2017, pp. 30-37, <http://dx.doi.org/10.1016/j.optmat.2017.04.005>.